International Scholarly Research Network
ISRN Mechanical Engineering
Volume 2011, Article ID 727120, 13 pages
doi:10.5402/2011/727120

Research Article

Vibration Analysis of a Rotating Disk with a Crack

A. S. Bouboulas and N. K. Anifantis

Machine Design Laboratory, Mechanical and Aeronautics Engineering Department, University of Patras, 26500 Patras, Greece

Correspondence should be addressed to N. K. Anifantis, nanif@mech.upatras.gr

Received 3 May 2011; Accepted 15 June 2011

Academic Editor: K. Yasuda

This paper studies the vibrational behaviour of a rotating disk with a radially or circumferentially oriented crack. The disk rotates with a constant angular speed. To treat this problem, the finite element method is employed. The disk is discretised into finite elements, and the crack is considered as nonpropagating and always open. The solutions to this problem's governing equations yield the natural frequencies and mode shapes. The frequency response due to dynamic loading is also yielded to determine the crack's effect on the frequency domain. For both crack orientations, parametric studies are conducted to investigate the sensitivity of the vibrational behaviour to the disk's angular speed and radial crack length or circumferential crack angle and distance from the disk's centre. The accuracy of the results is validated through comparisons with results available from the literature.

1. Introduction

Rotating disks are the principal components in various rotating machinery applications, such as turbine blades, circular saws, and computer memory disks. The occurrence of cracks in a rotating disk induces local variations in the stiffness, the magnitude of which mainly depends on the location and depth of the cracks. These variations, in turn, have a significant effect on the vibrational behaviour of the entire rotating machinery. To ensure safe operation of rotating machinery, it is extremely important to know whether the components (such as the rotating disks) are free of cracks and to assess their extent if present. The procedures that are often used for detection are direct procedures, such as ultrasound, X-rays, and so forth. However, these methods have proven to be inoperative and unsuitable in certain cases because they require expensive and minutely detailed inspections. To avoid these disadvantages, during the last decades, researchers have focused on developing more efficient procedures for crack detection that are based on changes in the vibrational characteristics (natural frequencies, mode shapes, and modal damping values) introduced by the crack [1]. Different techniques to model a crack in these procedures are presented by Dimarogonas [2].

Several studies have focused on the vibrational behaviour of uncracked rotating disks. As early as 1921, Lamb and Southwell [3] determined the natural frequencies of a flexible rotating disk, which neglected the bending effects. Kirkhope and Wilson [4] calculated the natural frequencies of a thin axisymmetric rotating disk by employing efficient annular finite elements. Liang et al. [5] investigated the natural frequencies of a spinning polar orthotropic disk that was subjected to a stationary concentrated transverse load. Chung et al. [6] analysed the nonlinear dynamic response of a flexible spinning disk with angular acceleration. In later works, Chung and his coworkers [7, 8] studied the effects of misalignment between the axes of symmetry and rotation on the natural frequencies and mode shapes of a flexible rotating disk. Baddour and Zu [9] presented and analysed an approximate solution to the nonlinear coupled vibrations of a spinning disk, which included the in-plane inertia of the disk. Bashmal et al. [10] investigated the natural frequencies and mode shapes for the in-plane vibration of a circular disk under combinations of all possible classical boundary conditions. Ranjan and Ghosh [11] studied the effect of discrete point masses and distributed patches of masses on the natural frequencies, mode shapes, and response due to an external excitation for the case of a spinning disk.

The problem of a rotating disk with a crack has attracted the interest of several researchers. Rooke and Tweed [12] considered the elastic problem of a finite rotating elastic disk with a radial crack. The stress intensity factor and crack energy were determined in terms of a solution to the Fredholm integral equation. Smith [13] calculated the stress intensity factors of an arc crack in a rotating disk by using two distinct boundary element approaches. Schneider and Danzer [14] employed a closed-form weight function to calculate the stress intensity factor of an edge crack in a finite elastic disk. Shariati et al. [15] developed a formula to predict the stress intensity factor of a radial crack in a rotating disk. Jia and Lee [16] presented an analytical relation between the distributed imperfections (nonuniform thickness, density, Young's modulus, Poisson's ratio, and the odd distribution of internal stresses) of a rotating circular disk and the resulting split modes. Raman and Mote [17] studied experimentally the nonlinear vibrations of an imperfect disk that was spinning near critical speed. Gyekenyesi and his coworkers [18, 19] presented a vibration-based crack detection method for rotating disks. They considered that the presence of a crack distorts the strain field within the disk. Consequently, measurable deformation in the disk's geometry and a corresponding change in the system's centre of mass occurred. However, the results show this study's failure to identify the existence of the crack. Based on the above-cited references, a limited number of studies are available in the literature on the vibrational behaviour of cracked rotating disks.

This study constitutes a primary approach for the vibrational behaviour of a cracked disk that is rotating with a constant angular speed. The radially or circumferentially oriented crack (through the full thickness of the disk) is considered to be nonpropagating and always open, whereas the disk is discretised into finite elements. Based on Lagrange's equation, the finite element equations of this model are obtained. The effect of Coriolis term, proportional to angular speed, on the disk vibrational behavior is not significant, since it is assumed that the disk does not rotate at very high speeds. For reasons of solution simplicity, the Coriolis term is neglected in this study. The governing equations of this linear vibrational problem are expressed in time domain, since neither crack detection techniques nor signal analysis is involved in this study. The main objective of this study is to investigate the difference of vibrational behaviour between the uncracked and cracked disk. Based on the eigenvalue and harmonic analyses, the natural frequencies, mode shapes, and frequency response due to dynamic loading are obtained. Although it is not the main objective of this study, stability analysis is performed and the critical speed is extracted. For both crack orientations, parametric studies are carried out to investigate the sensitivity of the natural frequencies, mode shapes with respect to the disk's angular speed and radial crack length or circumferential crack angle and distance from the disk's centre. The influence of crack's characteristics (orientation, position, and depth) on the critical speed is also studied. The accuracy of the results is demonstrated through comparisons with results available in the literature. Observations are made to determine the utility of this method in crack detection techniques.

2. Finite Element Procedure

The following discussion considers a cracked disk that rotates with a constant angular speed. The disk's material properties are considered to be linear elastic, and the displacements and strains are assumed to be small. The crack is considered as nonpropagating and always open, and the disk is discretised into a set of conventional finite elements. The equations of this problem are formulated based on the well-known generalised problem of rotating bladed disks [20]. For reasons of completeness, this generalised problem is briefly presented below and adapted to the present study by ignoring any nonlinearities due to the rotating blades.

Figure 1 illustrates a disk that is clamped at the inner radius R_i and free at the outer radius R_o. The disk contains a radial or circumferential crack through the full thickness of the disk. The radial crack has length a and terminates at the outer radius of the disk. The internal circumferential crack subtends an angle θ and is located at a distance R from the disk's centre. The morphology of the disk model is designed in a way that allows for changes in crack geometry. Thus, by considering the radial crack length a or circumferential crack angle θ and the distance R as global design variables, parametric studies are possible. The disk rotates about the Z axis of an inertial coordinate system (X, Y, Z) with a constant angular speed ω (Figure 1). The inertial co-ordinate system is fixed to the disk's centre. The X and Y axes lie along the horizontal and vertical symmetry axes of the disk, respectively, and the Z axis is perpendicular to the disk (Figure 1). The crack is considered to be nonpropagating and always open. The domain of the disk is discretised into a layer of three-dimensional finite elements. Figure 2 shows the finite element meshes for a disk with a radial or circumferential crack. For both crack orientations, the disk is discretised into eight-node isoparametric hexahedral finite elements. Each node of such an element has three degrees of freedom that represent the nodal displacements along the three dimensions. Similar finite element meshes have been developed for all of the considered crack cases in this study.

Consider an element in the finite element mesh shown in Figure 2. The position vector $\mathbf{r}$, displacement vector $\mathbf{u}$, and velocity vector $\dot{\mathbf{u}}$ of a material point that is located in the element are [21] as follows:

$$\mathbf{r} = \mathbf{N}\mathbf{c}, \qquad \mathbf{u} = \mathbf{N}\mathbf{q}, \qquad \dot{\mathbf{u}} = \mathbf{N}\dot{\mathbf{q}}, \tag{1}$$

where $\mathbf{N}$ is the shape function matrix, $\mathbf{c}$ is the element's nodal coordinates vector, $\mathbf{q}$ is the element's nodal displacement vector, and $\dot{\mathbf{q}}$ is the element's nodal velocity vector. The vectors and matrix of (1) are defined with respect to a local co-ordinate system (x, y, z) that rotates about the Z axis. The vectors $\mathbf{c}, \mathbf{q}$, and $\dot{\mathbf{q}}$ are of order 24, and the matrix $\mathbf{N}$ is of order 3×24.

The corresponding strain vector $\boldsymbol{\varepsilon}$ and stress vector $\boldsymbol{\sigma}$ of the material point are as follows [21]:

$$\boldsymbol{\varepsilon} = \mathbf{B}\mathbf{q}, \qquad \boldsymbol{\sigma} = \mathbf{D}\varepsilon, \tag{2}$$

where $\mathbf{B}$ is the strain-displacement matrix of order 6×24, and $\mathbf{D}$ is material stiffness matrix of order 6×24.

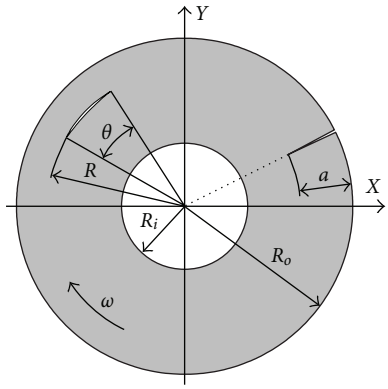

Figure 1: Disk model with a radial or circumferential crack.

The absolute velocity $\mathbf{v}$ of the material point is given by the following [20]:

$$\mathbf{v} = \dot{\mathbf{u}} + \boldsymbol{\Omega}(\mathbf{r} + \mathbf{u}), \tag{3}$$

where

$$\boldsymbol{\Omega} = \omega \begin{bmatrix} 0 & -1 & 0 \\ 1 & 0 & 0 \\ 0 & 0 & 0 \end{bmatrix}. \tag{4}$$

The kinetic energy of the element is as follows:

$$T = \frac{1}{2} \int_V \rho \mathbf{v}^{\mathrm{T}} \mathbf{v} \, \mathrm{d}V, \tag{5}$$

where ρ is the material density, and V is the volume of the element. By substituting (3) and (1) into (5), the kinetic energy can be written as follows:

$$\begin{aligned} T = {} & \frac{1}{2} \int_V \rho \dot{\mathbf{q}}^{\mathrm{T}} \mathbf{N}^{\mathrm{T}} \mathbf{N} \dot{\mathbf{q}} \, \mathrm{d}V + \frac{1}{2} \int_V \rho \mathbf{c}^{\mathrm{T}} \mathbf{N}^{\mathrm{T}} \boldsymbol{\Omega}^2 \mathbf{N} \mathbf{c} \, \mathrm{d}V \\ & + \frac{1}{2} \int_V \rho \mathbf{q}^{\mathrm{T}} \mathbf{N}^{\mathrm{T}} \boldsymbol{\Omega}^2 \mathbf{N} \mathbf{q} \, \mathrm{d}V + \int_V \rho \dot{\mathbf{q}}^{\mathrm{T}} \mathbf{N}^{\mathrm{T}} \boldsymbol{\Omega} \mathbf{N} \mathbf{c} \, \mathrm{d}V \\ & + \int_V \rho \mathbf{c}^{\mathrm{T}} \mathbf{N}^{\mathrm{T}} \boldsymbol{\Omega}^2 \mathbf{N} \mathbf{q} \, \mathrm{d}V \int_V \rho \, \dot{\mathbf{q}}^{\mathrm{T}} \mathbf{N}^{\mathrm{T}} \boldsymbol{\Omega} \mathbf{N} \mathbf{q} \, \mathrm{d}V, \end{aligned} \tag{6}$$

where $\boldsymbol{\Omega}^2 = \boldsymbol{\Omega}^{\mathrm{T}} \boldsymbol{\Omega}$.

The potential energy of the element is as follows:

$$U = \frac{1}{2} \int_V \boldsymbol{\varepsilon}^{\mathrm{T}} \boldsymbol{\sigma} \, \mathrm{d}V. \tag{7}$$

By substituting (2) into (7), the potential energy can be written as follows:

$$U = \frac{1}{2} \int_V \mathbf{q}^{\mathrm{T}} \mathbf{B}^{\mathrm{T}} \mathbf{D} \mathbf{B} \mathbf{q} \, \mathrm{d}V. \tag{8}$$

To derive the linear dynamic equations at the elemental level, Lagrange's equation is employed:

$$\frac{\mathrm{d}}{\mathrm{d}t} \left(\frac{\partial T}{\partial \dot{\mathbf{q}}} \right) - \frac{\partial T}{\partial \mathbf{q}} + \frac{\partial U}{\partial \mathbf{q}} = \mathbf{f}_{\mathrm{ext}}. \tag{9}$$

By considering that the matrix $\boldsymbol{\Omega}$ is time independent and by substituting (6) and (8) into (9), the equations of motion at the elemental level can be written in compact form

$$\mathbf{m}\ddot{\mathbf{q}} + \mathbf{c}_c \dot{\mathbf{q}} + (\mathbf{k}_e - \mathbf{k}_r)\mathbf{q} + \mathbf{f}_e = \mathbf{f}_{\mathrm{ext}}, \tag{10}$$

where $\mathbf{m}$ is the element's mass matrix, $\ddot{\mathbf{q}}$ is the element's nodal acceleration vector, $\mathbf{c}_c$ is the element's Coriolis damping matrix, $\mathbf{k}_e$ is the element's stiffness matrix, $\mathbf{k}_r$ is the element's centrifugal stiffness matrix, $\mathbf{f}_e$ is the element's rotational force vector, and $\mathbf{f}_{\mathrm{ext}}$ is the element's external load vector. The matrices of (10) have dimensions of 24×24, and the vectors have a dimension of 24. The matrices and vector definitions of (10) are as follows:

$$\begin{gathered} \mathbf{m} = \int_V \rho \mathbf{N}^{\mathrm{T}} \mathbf{N} \, \mathrm{d}V, \qquad \mathbf{c}_c = 2 \int_V \rho \mathbf{N}^{\mathrm{T}} \boldsymbol{\Omega} \mathbf{N} \, \mathrm{d}V, \\ \mathbf{k}_e = \int_V \mathbf{B}^{\mathrm{T}} \mathbf{D} \mathbf{B} \, \mathrm{d}V, \end{gathered} \tag{11a}$$

$$\mathbf{k}_r = \int_V \rho \mathbf{N}^{\mathrm{T}} \boldsymbol{\Omega}^2 \mathbf{N} \, \mathrm{d}V, \qquad \mathbf{f}_e = -\int_V \rho \mathbf{N}^{\mathrm{T}} \boldsymbol{\Omega}^2 \mathbf{N} \mathbf{c} \, \mathrm{d}V. \tag{11b}$$

After assembly and without considering the slight effect of structural damping, the equilibrium equations that govern the linear dynamic response of the discretised cracked rotating disk are as follows:

$$\mathbf{M}\ddot{\mathbf{Q}} + \mathbf{C}_c \dot{\mathbf{Q}} + (\mathbf{K}_e - \mathbf{K}_r)\mathbf{Q} + \mathbf{F}_e = \mathbf{F}_{\mathrm{ext}}, \tag{12}$$

where $\mathbf{M}$ is the global mass matrix, $\mathbf{C}_c$ is the global Coriolis damping matrix, $\mathbf{K}_e$ is the global stiffness matrix, $\mathbf{K}_r$ is the global centrifugal stiffness matrix, $\ddot{\mathbf{Q}}$ is the global acceleration vector, $\dot{\mathbf{Q}}$ is the global velocity vector, $\mathbf{Q}$ is the global displacement vector, $\mathbf{F}_e$ is the global rotational force vector, and $\mathbf{F}_{\mathrm{ext}}$ is the global external load vector. The definitions of these global matrices and vectors are as follows:

$$\mathbf{X} = \mathop{\mathbf{A}}_{i=1}^{N} \mathbf{x}, \tag{13}$$

where $\mathbf{X}$ represents the global matrices and vectors of (12), $\mathbf{x}$ denotes the corresponding matrices and vectors of (10), $\mathbf{A}$ stands for the assembly operator, and N represents the number of discretised elements. The global matrices and vectors of (12) have dimensions $N_{\mathrm{dof}} \times N_{\mathrm{dof}}$ and N_{dof}, respectively, where N_{dof} denotes the degrees of freedom of the finite element mesh. Because vector $\mathbf{F}_e$ is time independent, it is moved to the right side of (12) and is treated as an external force. Furthermore, it is assumed that the disk does not rotate at very high angular speed (two times the first natural frequency of stationary disk). Thus, the influence of Coriolis term, $\mathbf{C}_c$, on (12) is not significant [22, 23]. To simplify the solution of (12), the Coriolis term is ignored. Based on the above, (12) can be written as follows:

$$\mathbf{M}\ddot{\mathbf{Q}} + (\mathbf{K}_e - \mathbf{K}_r)\mathbf{Q} = \mathbf{F}, \tag{14}$$

where $\mathbf{F} = \mathbf{F}_{\mathrm{ext}} - \mathbf{F}_e$. To derive the frequency response from (14), harmonic analysis is performed [24].

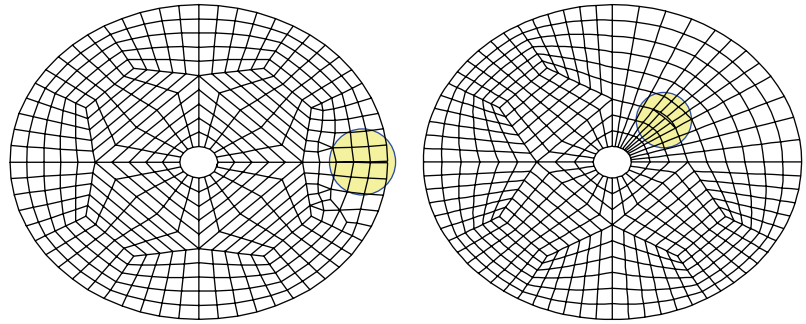

(a) (b)

Figure 2: Finite element mesh of a disk with (a) a radial crack of length $a/R_o = 0.3$ or (b) a circumferential crack of angle $\theta = 24^\circ$ at a distance $R/R_o = 0.4$.

Based on (14), the free vibration problem of the discretised cracked rotating disk is described as follows:

$$\mathbf{M}\ddot{\mathbf{Q}} + (\mathbf{K}_e - \mathbf{K}_r)\mathbf{Q} = \mathbf{0}. \tag{15}$$

To solve (15), eigenvalue analysis is performed [24]. Thus, the mode shapes $\boldsymbol{\phi}_{c(m,n)}$ with $m = 0, 1, 2, \ldots$ nodal circles and $n = 0, 1, 2, \ldots$ nodal diameters as well as the corresponding circular frequencies of vibration $\omega_{c(m,n)}$ (rad/sec) are obtained. Subscript c denotes the cracked state of the disk. The natural frequencies $f_{c(m,n)}$ are defined as $\omega_{c(m,n)} = 2\pi f_{c(m,n)}$. For reasons of simplicity, the solutions to (14) and (15) are implemented by using finite element codes.

3. Numerical Results and Discussions

In this section, the proposed study is applied to the disk model of Figure 1. This model has inner radius $R_i = 18.8468 \times 10^{-3}$ m, outer radius $R_o = 188.468 \times 10^{-3}$ m, thickness $h = 2.413 \times 10^{-3}$ m, modulus of elasticity $E = 62.5$ GPa, mass density $\rho = 2777\,\text{kg/m}^3$, and Poisson's ratio $\nu = 0.29$. The selected model's geometric and material properties correspond to the properties of a commercial cutting disk. Parametric studies implemented to investigate the sensitivity of the vibrational behaviour with respect to the disk's angular speed ω (varied from 0 Hz to 100 Hz with an increment of 8.33 Hz) and radial crack's dimensionless length a/R_o (varied from 0.15 to 0.9 with an increment 0.15) or circumferential crack's angle θ (varied from 12° to 36° with an increment 6°) and dimensionless distance R/R_o (varied from 0.2 to 0.8 with an increment 0.2). The influence of crack's characteristics (orientation, position, and depth) on the critical speed is also investigated. As previously mentioned, the disk is discretised into eight-node isoparametric hexahedral finite elements. Two typical meshes are illustrated in Figure 2: the first mesh is a radially cracked disk of $a/R_o = 0.3$, and the second mesh is a circumferentially cracked disk of $\theta = 24^\circ$ and $R/R_o = 0.4$. For all of the crack cases in this study, the disk's finite element meshes are composed of approximately the same number of nodes and elements. For example, when the disk contains a radial crack of $a/R_o = 0.3$, the finite element mesh consists of $N = 501$ eight-node isoparametric hexahedral finite elements and $N_{\text{dof}} = 1145$ nodes. For the uncracked disk, the finite element mesh is composed of $N = 500$ eight-node isoparametric hexahedral finite elements and $N_{\text{dof}} = 1080$ nodes. Convergence studies show that finer finite element meshes affect the results less than 1%. The solution to (15) yields the mode shapes $\boldsymbol{\phi}_{c(m,n)}$ and the associated natural frequencies $f_{c(m,n)}$ for the cracked rotating disk. In this study, the four lower natural frequencies and the corresponding mode shapes are considered where $m = 0$ and $n = 0, 1, 2, 3$.

Based on the deformed mesh of the employed finite element codes, the mode shapes $(0,1)$, $(0,2)$, and $(0,3)$ of the radially cracked rotating disk were observed to split into two different frequencies. One frequency corresponds to the symmetric mode shapes about the XZ plane of the inertia co-ordinate system and the other to the antisymmetric mode shapes about the same plane. The mode shape $(0,0)$ appears symmetric about the XZ plane and possesses a single natural frequency. Thus, the radial crack plays a role of asymmetry, in some, but not all mode shapes of the disk. More detailed discussions about the symmetric and asymmetric mode shapes can be found in [25]. For example, Figures 3, 4, 5, and 6 illustrate the mode shapes of the disk with a radial crack of $a/R_o = 0.6$ and $\omega = 50$ Hz. For the circumferentially cracked rotating disk, the mode shapes $(0,1), (0,2)$, and $(0,3)$ possess two identical natural frequencies, and the mode shape $(0,0)$ possesses a single natural frequency. All of these mode shapes are symmetric about the XZ plane. The solution to equation (14) provides the frequency response of the cracked rotating disk due to transverse impulse loading of 100 N that was applied at point A, which is located at the outer radius of the disk. Initially, the disk is stationary and undeformed. The transverse acceleration response at node B is extracted. The later node is located on the disk's outer diameter and is diametrically opposite from A. For verification, the stationary cracked, stationary uncracked, and rotating uncracked disks are considered. The eigenproblem and linear dynamic problem for the stationary cracked disk are described by (15) and (14), respectively, by neglecting any terms that are related to the rotation of the disk, ($\mathbf{K}_r = \mathbf{0}$), and are solved as the corresponding problems of the cracked rotating disk. The derived mode shapes for both crack orientations appear either symmetric

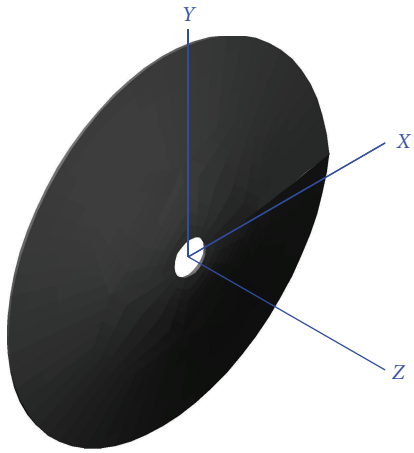

Figure 3: The symmetric mode shape $(0,0)$ for a rotating disk ($\omega = 50$ Hz) with a radial crack of length $a/R_o = 0.6$. The corresponding natural frequency is $f_{c(0,0)} = 79.8$ Hz.

or antisymmetric about the XZ plane as the corresponding mode shapes of the rotating cracked disk. Comparisons show that the mode shapes of the stationary cracked disk have similar forms to the corresponding mode shapes of the rotating cracked disk. The values of the natural frequencies for the stationary cracked disk are lower than the values of the rotating cracked disk. The equations that govern the eigenproblem and the linear dynamic problem of the rotating uncracked disk are of the same type as (15) and (14), respectively, and are solved as the cracked rotating disk. Any difference with respect to (15) and (14) caused due to the uncracked disk's finite element mesh data (number of nodes and elements). By neglecting any terms that are related to the rotation of the uncracked disk in this problem, ($\mathbf{K}_r = \mathbf{0}$), the equations for the stationary uncracked disk are obtained. For both stationary and rotating uncracked disks, the symmetric mode shapes $(0,1)$, $(0,2)$, and $(0,3)$ possess two identical natural frequencies, whereas the symmetric mode shape $(0,0)$ possesses a single natural frequency. The mode shapes of the rotating uncracked disk have similar form to the mode shapes of the stationary uncracked disk. The values of the natural frequencies for the stationary uncracked disk are lower than the values of the rotating uncracked disk. Since the implementation of very expensive and time-consuming experiments is out of the scope of this study, the results presented below are compared with any numerical results available from the literature and analytical results. An accuracy study is performed for the stationary uncracked disk. The natural frequencies $f_{u(m,n)}$, which were obtained from the corresponding eigenproblem, are 66, 54.2, 87.3 and 193.2 Hz for $m = 0$ and $n = 0,1,2,3$, respectively. Subscript u denotes the stationary uncracked disk. Comparisons are performed with the corresponding analytical natural frequencies $f^*_{u(m,n)}$ [26], where $*$ represents the analytical results. The absolute percentage differences $((f_{u(m,n)} - f^*_{u(m,n)})/f^*_{u(m,n)}) \times 100$ of these natural frequencies lie between 0.1% for the natural frequency of the symmetric mode shape $(0,1)$ and 0.2% for the natural frequency of the symmetric mode shape $(0,3)$. Thus, the results of this study are very close to the analytical ones. This accuracy study was also performed by using $f_{u(m,n)}$, which are the natural frequencies obtained from the transverse acceleration frequency response. Comparisons are performed with the analytical natural frequencies $f^*_{u(m,n)}$ noted above. The absolute percentage differences of these natural frequencies lie between 0.8% for the natural frequency of the symmetric mode shape $(0,1)$ and 2.9% for the natural frequency of the symmetric mode shape $(0,3)$. Thus, the results that were obtained by using the frequency response are close to the analytical values. Comparisons with the previous study show that the accuracy of the natural frequencies, which were obtained with the eigenproblem, is higher than those obtained from frequency response. An accuracy study has also been performed for the rotating uncracked disk, since, according to the author's knowledge, no results are available in the literature related to the vibrational behaviour of a cracked rotating disk. Based on the corresponding eigenproblem, the three lower natural frequencies ($m = 0$ and $n = 0,1,2$) of the uncracked disk rotating at $\omega = 83.33$ Hz are 95, 103.4 and 154.5 Hz, respectively. Comparisons are performed with the analytical results of [27]. The absolute percentage differences of these symmetric natural frequencies lie between 3.3% for the natural frequency of mode shape $(0,0)$ and 4.9% for the natural frequency of mode shape $(0,3)$. Thus, the results of this study are in good agreement with analytical results.

3.1. Stationary Disk. Figure 7 illustrates the variations in the stationary disk's natural frequencies $f_{c(m,n)}/f_{u(m,n)}$ for $m = 0$, $n = 0,1,2,3$ with a radial crack length of a/R_o. As it is expected [28], the presented natural frequencies decrease as the crack length increases. For small values of crack depth ($a/R_o \leq 0.15$), the natural frequencies generally change slightly. For $a/R_o \geq 0.2$, the natural frequencies of symmetric mode shapes $(0,2)$ and $(0,3)$ appear to have higher values than the corresponding natural frequencies of the antisymmetric mode shapes $(0,2)$ and $(0,3)$. On the contrary, for $a/R_o \geq 0.5$, the natural frequency of the symmetric mode shape $(0,1)$ has a lower value than the corresponding natural frequency of the antisymmetric mode shape $(0,1)$. It also seems from Figure 7 that the natural frequencies of the antisymmetric mode shapes $(0,2)$ and $(0,3)$ are generally the most sensitive frequencies to variations in the crack length, whereas the natural frequency of the antisymmetric mode shape $(0,1)$ is less sensitive. Table 1 shows the four lower natural frequencies for a free-free stationary disk with a radial crack of $a/R_o = 0.9$. To obtain these results, the disk model of Figure 1 is slightly modified so that the boundary conditions at the inner radius are free. This problem is treated as the problem of the clamped-free stationary cracked disk. From Table 1, it seems that the results of this study are generally in good agreement with the corresponding numerical results that are reported in [28]. It is clarified that the results presented below are referred to the clamped-free disk of Figure 1. Based on the corresponding eigenproblem, the natural frequencies

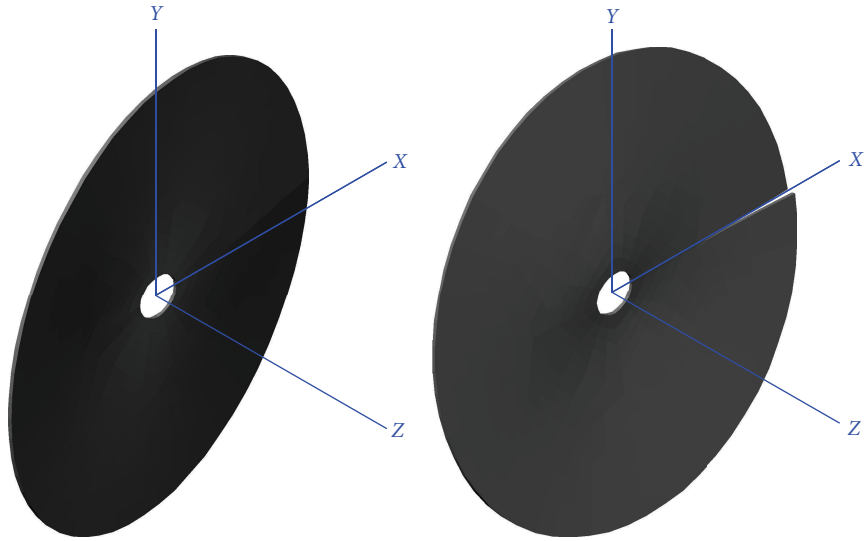

(a) (b)

Figure 4: Mode shape $(0, 1)$ for a rotating disk ($\omega = 50$ Hz) with a radial crack of length $a/R_o = 0.6$. (a) The symmetric mode with a natural frequency of 76 Hz and (b) the antisymmetric mode with a natural frequency of 75.4 Hz.

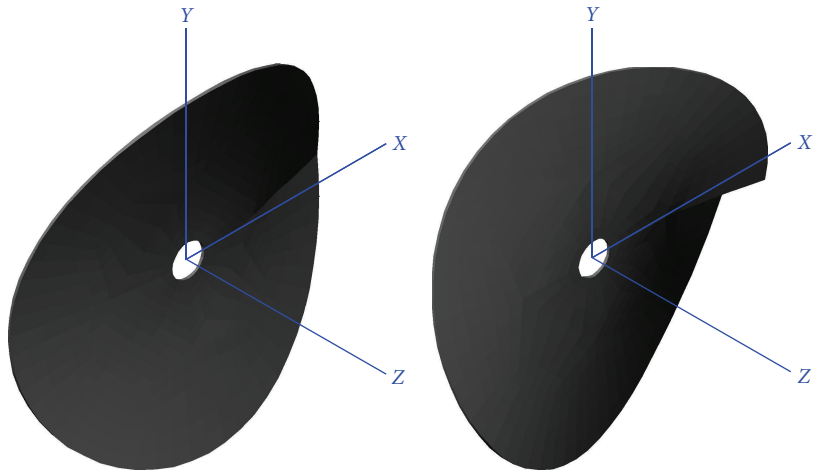

(a) (b)

Figure 5: Mode shape $(0, 2)$ for a rotating disk ($\omega = 50$ Hz) with a radial crack of length $a/R_o = 0.6$. (a) The symmetric mode with a natural frequency of 107.5 Hz and (b) the antisymmetric mode with a natural frequency of 103 Hz.

$f_{c(m,n)}/f_{u(m,n)}$, for $m = 0, n = 0, 1, 2, 3$ have also been calculated for a stationary disk with a circumferential crack. For all of the considered circumferential cracks in this study, all of the dimensionless natural frequencies ($m = 0$, $n = 0, 1, 2, 3$) approach one. Similar conclusions are reported in the literature, even for a crack of angle $\theta = 180^\circ$ that is located at different positions on the disk [29]. Comparisons show that the mode shapes of the uncracked disk have similar forms to the corresponding mode shapes of the circumferentially cracked disk.

Figure 8 depicts the transverse acceleration frequency responses for the stationary disk with a radial crack of two different lengths. For clarity, the corresponding response of the stationary uncracked disk is not plotted in this figure. However, in this and other similar figures presented below, the three vertical dashed lines represent the loci of the two identical natural frequencies for symmetric mode shapes $(0, 1)$, $(0, 2)$, and $(0, 3)$ of the stationary uncracked disk, and the solid line is the loci of the corresponding single natural frequency for the symmetric mode shape $(0, 0)$. These natural frequencies are evaluated from the transverse acceleration frequency response and are $54.1, 87.9, 187.4$ for mode shapes $(0, 1)$, $(0, 2)$, and $(0, 3)$ and 66.5 Hz for mode shape $(0, 0)$. The transverse acceleration frequency response for $a/R_o = 0.3$ exhibits four peaks that correspond to the natural frequencies of the symmetric mode shapes $(0, 1)$, $(0, 0)$, $(0, 2)$, and $(0, 3)$, respectively. The corresponding peaks for $a/R_o = 0.75$ appear at lower values of the

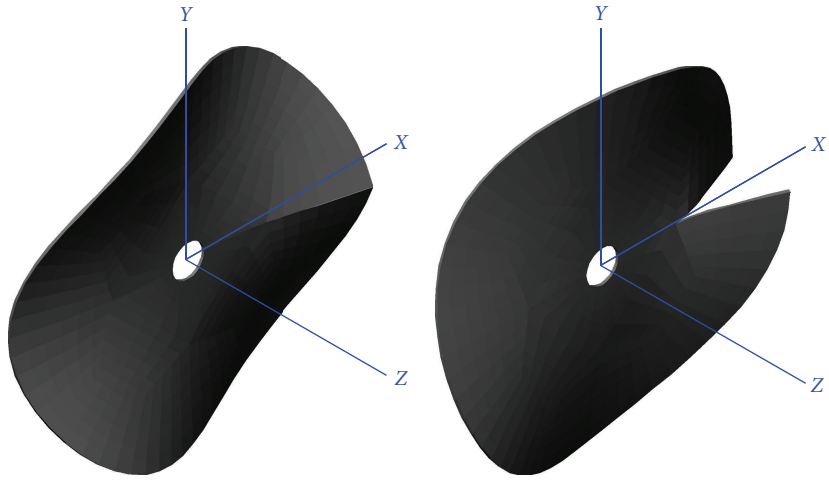

FIGURE 6: Mode shape (0, 3) for a rotating disk ($\omega = 50$ Hz) with a radial crack of length $a/R_o = 0.6$. (a) The symmetric mode with a natural frequency of 196.6 Hz and (b) the antisymmetric mode with a natural frequency of 171.2 Hz.

frequencies. Thus, the increase in the radial crack length causes the natural frequency to decrease. Similar conclusions were extracted from the eigenvalue analysis of Figure 7. It is also visible from Figure 8 that the natural frequencies of the symmetric mode shapes (0, 1), (0, 0), and (0, 2) for both values of the crack length are lower than the frequencies of the corresponding mode shapes for the stationary uncracked disk. Based on Figure 8, the absolute percentage differences in the natural frequencies for the two different values of the crack length lie between 2.7% for the natural frequency of the symmetric mode shape (0, 1) and 6.9% for the natural frequency of the symmetric mode shape (0, 3). From the eigenvalue analysis of Figure 7, these absolute percentage differences lie between 4.7% for the natural frequency of the symmetric mode shape (0, 1) and 7.1% for the natural frequency of the symmetric mode shape (0, 3). Thus, the results that were obtained from the frequency response are in good agreement with the results from the eigenvalue analysis. The peak, which is marked in Figure 8 with the symbol ¤, denotes the natural frequencies of the antisymmetric mode shape (0, 3) for $a/R_o = 0.75$. The transverse acceleration frequency response has also been evaluated for the case of a stationary disk with a circumferential crack. For all of the considered circumferential crack cases in this study, the presence of the crack very slightly affects all of the frequencies. Similar conclusions where reported above from the eigenvalue analysis.

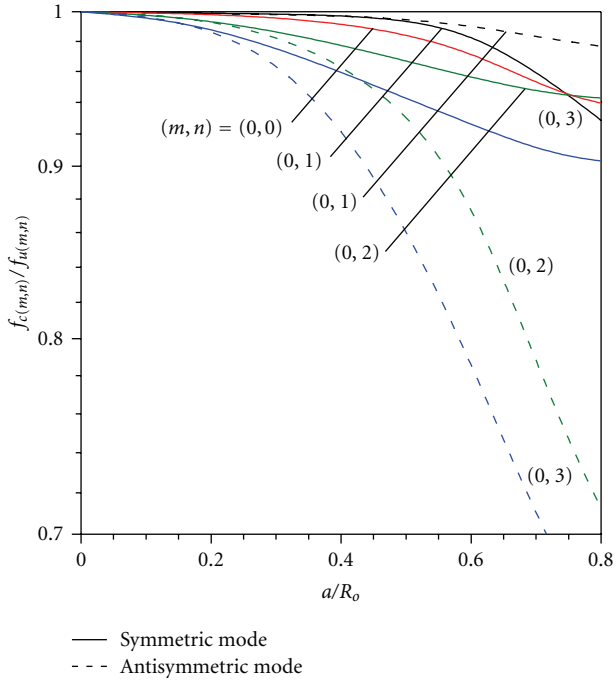

FIGURE 7: Variations in the four lower dimensionless natural frequencies for a stationary disk versus the radial crack's dimensionless length a/R_o.

3.2. Rotating Disk. Figure 9 presents the variation of the natural frequencies $f_{c(m,n)}$, $m = 0, n = 0, 1, 2, 3$, in terms of the angular speed ω for a disk with a radial crack of $a/R_o = 0.75$. It seems that for all of the considered angular speed values, the natural frequencies of this figure increase with the angular speed. Based on (4), (11b), (13) and (15), it is deduced that the global centrifugal stiffness matrix $\mathbf{K}_r$ is proportional to the second-order angular speed ω^2 and is always negative. Thus, the presence of this negative term in the (15) increases the structural stiffness matrix causing in turn an increase of the natural frequencies with angular speed. Similar conclusions concerning the effect of the global centrifugal stiffness matrix are reported in literature [11, 30]. Figure 9 shows that the natural frequencies of the symmetric mode shape (0, 3) appear to have the highest value in comparison to the other frequencies in this figure. Furthermore, the natural frequencies of the symmetric mode shapes (0, 2) and (0, 3) get higher values than the

Table 1: The four lower dimensionless natural frequencies of a free-free stationary disk with a radial crack of dimensionless length $a/R_o = 0.9$.

	$f_{c(0,1)}/f_{u(0,1)}$	$f_{c(0,2)}/f_{u(0,2)}$	$f_{c(0,0)}/f_{u(0,0)}$	$f_{c(0,3)}/f_{u(0,3)}$
Symmetric mode				
Yuan et al., [28]	0.627	0.795	0.907	0.917
Present study	0.610	0.784	0.861	0.259
% Difference of natural frequency	2.641	1.412	5.089	1.178
Antisymmetric mode				
Yuan et al., [28]	0.262	0.468	0.584	0.685
Present study	0.259	0.457	0.538	0.622
% Difference of natural frequency	1.267	2.262	7.895	9.228

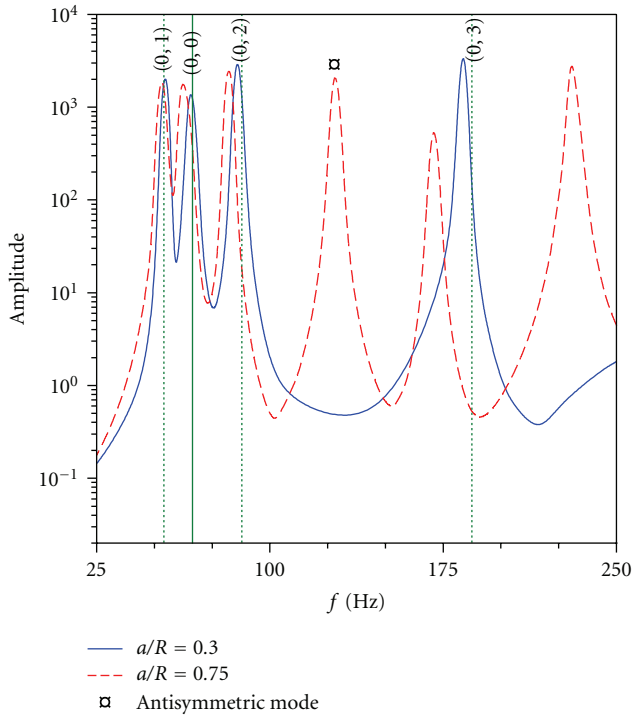

Figure 8: Frequency response of the stationary disk for two different radial cracks.

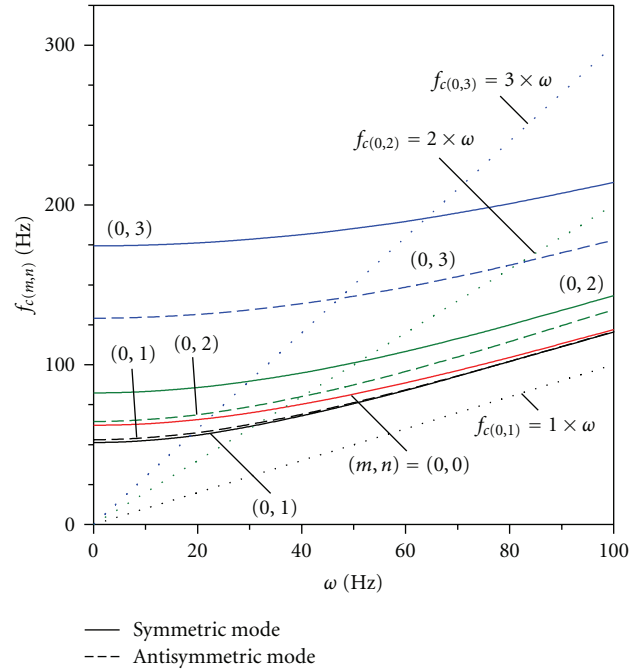

Figure 9: Variations in the natural frequencies versus the angular speed ω for a disk with a radial crack of $a/R_o = 0.75$.

corresponding values of antisymmetric mode shapes $(0, 2)$ and $(0, 3)$. On the contrary, the values of natural frequencies for both symmetric and antisymmetric mode shapes $(0, 1)$ nearly coincide. The dotted lines in Figure 9 are described by equations $f_{c(m,n)} = n \times \omega$, where n represents the number of nodal diameters for mode shape (m, n). The critical speed $\omega_{\mathrm{cr}(m,n)}$ for a mode shape (m, n) corresponds to the value of ω at which the line $f_{c(m,n)} = n \times \omega$ intersects with the natural frequency curve of mode shape (m, n) [7, 31]. It is observed from Figure 9 that the curves of both symmetric and antisymmetric mode shapes $(0, 1)$ do not intersect with the line of $f_{c(0,1)} = 1 \times \omega$. Thus, there are no critical speeds corresponding to both symmetric and antisymmetric mode shapes $(0, 1)$. The critical speeds for symmetric mode shapes $(0, 2)$, and $(0, 3)$ are 63 Hz and 50 Hz, respectively. The corresponding critical speeds for antisymmetric mode shapes $(0, 2)$, and $(0, 3)$ are 47 Hz and 40 Hz, respectively. The same study has been implemented to extract the critical speeds for all considered values of radial crack length, a/R_o, in this study (Figure 10). For all these values of crack length, there is no critical speed corresponding to both symmetric and antisymmetric mode shapes $(0, 1)$. Figure 10 depicts the critical speeds of both symmetric and antisymmetric mode shapes $(0, 2)$ and $(0, 3)$ versus radial crack length. It is observed that for $a/R_o \geq 0.2$, the critical speed corresponding to the symmetric mode shape $(0, 3)$ has highest value in comparison to the other critical speeds in this figure. For $a/R_o \geq 0.2$, the values of critical speed for symmetric mode shape $(0, 3)$ are higher than the corresponding values of antisymmetric mode shape $(0, 3)$. The differences between the values of these critical speeds increase as the radial crack length increases. Similar conclusions are extracted for

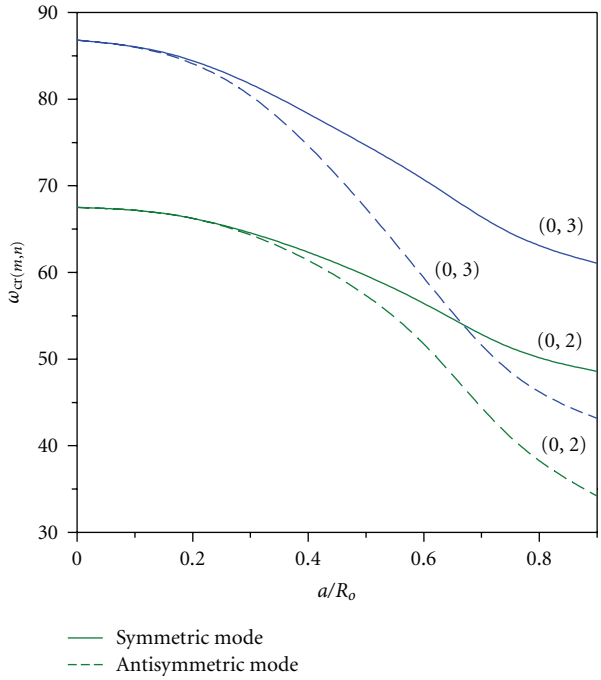

FIGURE 10: Variations in critical speeds for both symmetric and antisymmetric mode shapes $(0, 2)$ and $(0, 3)$ versus the dimensionless radial crack length a/R_o.

the values and differences of critical speed corresponding to symmetric and antisymmetric mode shapes $(0, 2)$, when $a/R_o \geq 0.3$. In what follows, the effect of the radial crack length of the natural frequencies of the rotating disk is studied. Figures 11 and 12 depict the variation in the four lower natural frequencies $f_{c(m,n)}/f_{u(m,n)}$ for $m = 0$, $n = 0, 1, 2, 3$ in terms of the angular speed ω for three different values of the radial crack length a/R_o. It is visible from Figure 11(a) that for $\omega < 30$ Hz, the natural frequency of the symmetric mode shape $(0, 0)$ for $a/R_o = 0.15$ gets higher values than the corresponding natural frequencies for $a/R_o = 0.6$ and $a/R_o = 0.9$. At $\omega = 30$ Hz, and the natural frequencies for all of the considered radial crack length values meet and become 1.1 times greater than the corresponding natural frequency of the stationary uncracked disk. For $30 < \omega \leq 100$, the values of the natural frequency for $a/R_o = 0.9$ are higher than the frequency values for $a/R_o = 0.15$ and $a/R_o = 0.6$. From Figure 11(b), it seems that the natural frequencies for $a/R_o = 0.15$ and $a/R_o = 0.6$ that correspond to the symmetric, and antisymmetric mode shapes $(0, 1)$ nearly coincide. It also presented that for $a/R_o = 0.9$, the values of the natural frequencies for antisymmetric mode shape $(0, 1)$ are higher than the corresponding values of the symmetric mode shape $(0, 1)$. The difference between the values of these two natural frequencies decreases slightly as the angular speed increases. For $\omega \leq 30$ Hz, the natural frequencies of the symmetric mode shape $(0, 1)$ for $a/R_o = 0.15$ and $a/R_o = 0.6$ appear to have the highest value in comparison to the other frequencies in this figure, whereas for $\omega > 30$ Hz, the antisymmetric mode shape $(0, 1)$ for $a/R_o = 0.9$ has the highest value. Based on Figure 12(a), it is observed that for $a/R_o = 0.15$, the natural frequencies for both symmetric and antisymmetric mode shapes $(0, 2)$ get higher values than the corresponding frequencies for $a/R_o = 0.6$ and $a/R_o = 0.9$. Also, for $a/R_o = 0.15$, the natural frequencies for the symmetric and antisymmetric mode shapes $(0, 2)$ coincide. For $a/R_o = 0.6$ and $a/R_o = 0.9$, the natural frequency values for the symmetric mode shape $(0, 2)$ are higher than the corresponding values for the antisymmetric mode shape $(0, 2)$. For $a/R_o = 0.6$, the differences between the frequencies of the antisymmetric and symmetric mode shapes $(0, 2)$ are nearly constant in terms of the angular speed, whereas the differences for $a/R_o = 0.9$ decrease as the angular speed increases. Figure 12(b) shows that for $a/R_o = 0.15$, the natural frequencies for both the symmetric and antisymmetric mode shapes $(0, 3)$ nearly coincide and get higher values than the corresponding frequencies for $a/R_o = 0.6$ and $a/R_o = 0.9$. The natural frequencies for the symmetric mode shape $(0, 3)$ of $a/R_o = 0.6$ and $a/R_o = 0.9$ get higher values than the corresponding natural frequencies of the antisymmetric mode shape $(0, 3)$. The differences between the values of the natural frequencies for the antisymmetric and symmetric mode shape for both $a/R_o = 0.6$ and $a/R_o = 0.9$ decrease slightly as the angular speed increases. Figure 13 illustrates the transverse acceleration frequency responses for a disk with a radial crack of two different lengths. For each crack case, two different values of the angular speed are considered. Figure 13(a) shows that the transverse acceleration frequency response for $\omega = 16.67$ Hz appears to have four peaks that correspond to the symmetric natural frequencies of mode shapes $(0, 1)$, $(0, 0)$, $(0, 2)$, and $(0, 3)$, respectively. The corresponding peaks for $\omega = 33.33$ Hz appear at higher frequency values. Thus, the increase in the angular speed causes increase in the natural frequencies. Similar conclusions were obtained from the eigenvalue analysis illustrated in Figures 11 and 12. Based on Figure 13(a), the absolute percentage differences in the natural frequencies for the two different angular speed values are 12.9%, 6.4%, 10.7%, and 3.9% for the natural frequencies of the symmetric mode shapes $(0, 0)$, $(0, 1)$, $(0, 2)$, and $(0, 3)$, respectively. For both angular speeds, the natural frequencies of the symmetric mode shapes differ with the corresponding frequencies of the stationary uncracked disk, which are shown in this figure by the vertical lines. The same study is implemented by considering a high crack length value ($a/R_o = 0.75$). Based on Figure 13(b), it seems that the increase in angular speed causes increase in the natural frequencies for the symmetric mode shapes $(0, 0)$, $(0, 1)$, $(0, 2)$, and $(0, 3)$. The absolute percentage differences in the natural frequencies for the two different values of the angular speed are 14.9%, 12.1%, 8.3%, and 3% for the natural frequencies of the symmetric mode shapes $(0, 0)$, $(0, 1)$, $(0, 2)$, and $(0, 3)$, respectively. The natural frequency of the antisymmetric mode shape $(0, 3)$, which is marked in Figure 13(b) with symbol ¤, also increases as the angular speed increases. The absolute percentage difference in this frequency for both values of the angular speed is 3.4%. The above study has also been implemented for the circumferentially cracked disk. It was deduced that the natural frequencies $f_{c(m,n)}$ with $m = 0$, $n = 0, 1, 2, 3$, which were obtained from the eigenproblem, are unaffected by the variation of the circumferential crack's angle θ and

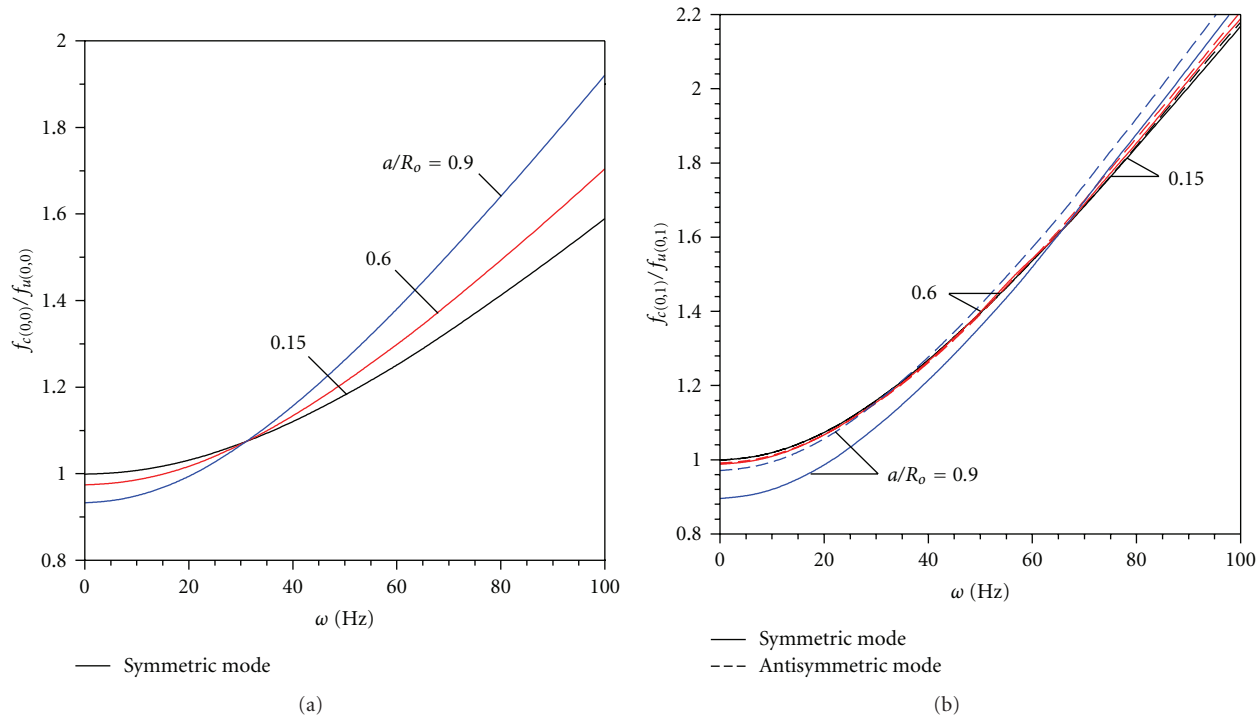

FIGURE 11: Variations in the dimensionless natural frequencies for mode shapes (a) $(0,0)$ and (b) $(0,1)$ versus the angular speed ω for three different values of the dimensionless radial crack length a/R_o.

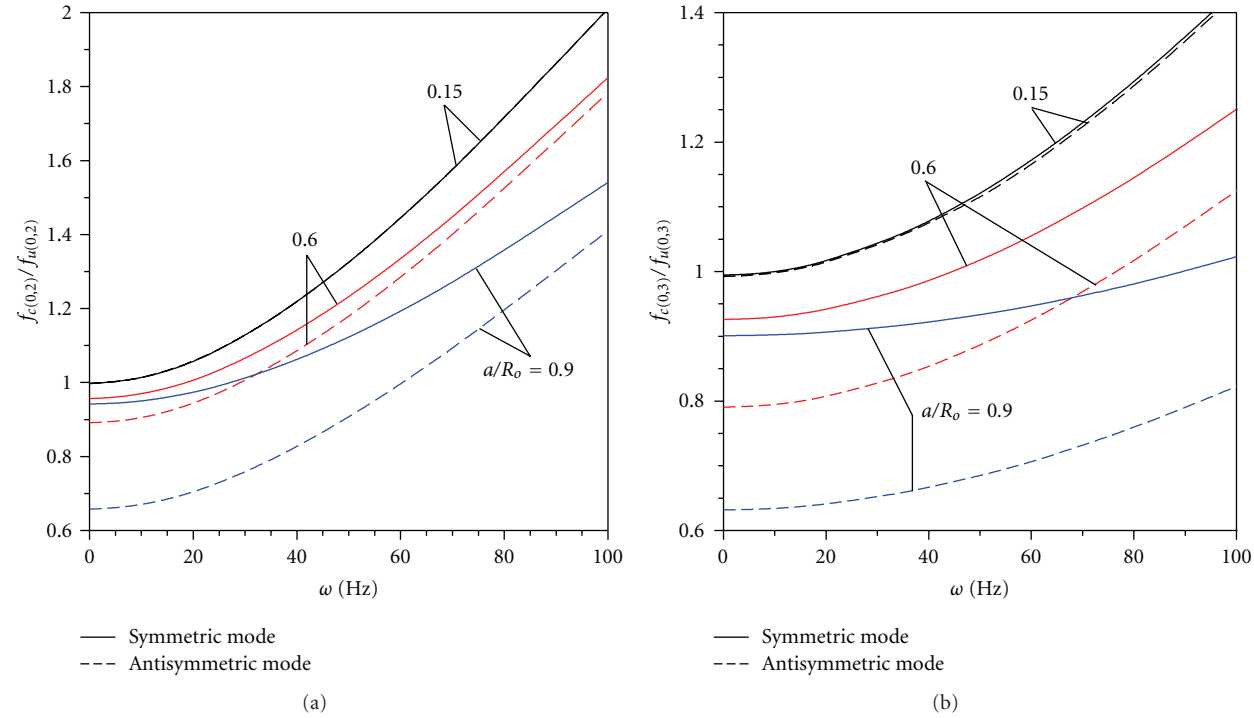

FIGURE 12: Variations in the dimensionless natural frequencies for mode shapes (a) $(0,2)$ and (b) $(0,3)$ versus the angular speed ω for three different values of the dimensionless radial crack length a/R_o.

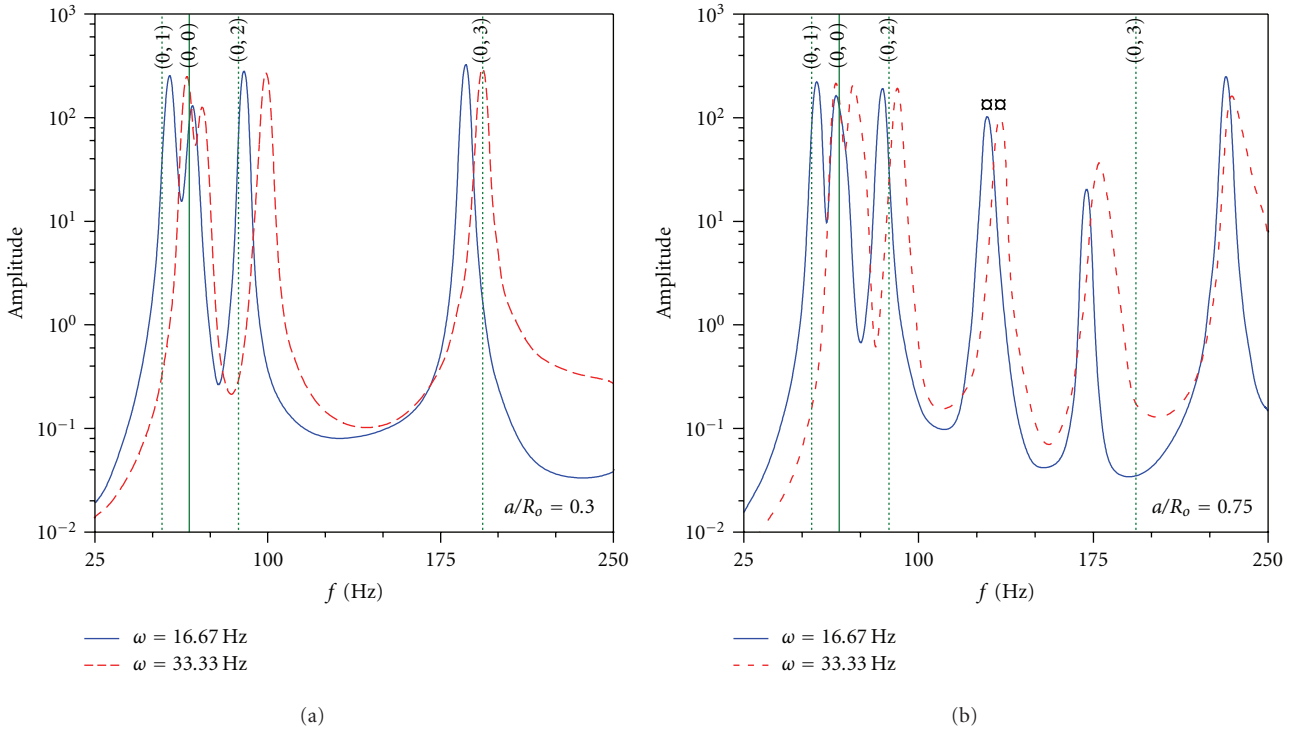

Figure 13: Frequency response of a disk with a radial crack of dimensionless length (a) $a/R_o = 0.3$ or (b) $a/R_o = 0.75$ and two different angular speed values.

dimensionless distance R/R_o. For all considered values of angular speed in this study, the values of natural frequencies of a circumferentially cracked disk are very close to the corresponding values of the uncracked rotating disk. Similar conclusions related to the values of natural frequencies were extracted from the transverse acceleration frequency response. Comparisons show that the mode shapes of the rotating disk with a circumferential crack have similar forms to the corresponding mode shapes of the rotating uncracked disk. Figure 14 shows the variation in the natural frequencies with the angular speed for a disk with a circumferential crack of $\theta = 24^\circ$ and $R/R_o = 0.4$. It seems that for all of the considered angular speed values, the natural frequencies of this figure increase with the angular speed. The values of the natural frequency for the mode shape $(0, 1)$ are higher than the frequencies of the other mode shapes, whereas the natural frequency of mode shape $(0, 3)$ gets the lowest values. The critical speeds were extracted based on the approach employed above for the radially cracked disk. It was observed that, critical speeds exist only for the mode shapes $(0, 2)$ and $(0, 3)$. For all considered values of circumferential crack's angle and dimensionless distance, the critical speeds are 67 Hz and 87 Hz, respectively. These values nearly coincide with the results of Figure 10 corresponding to rotating uncracked disk ($a/R_o = 0.0$).

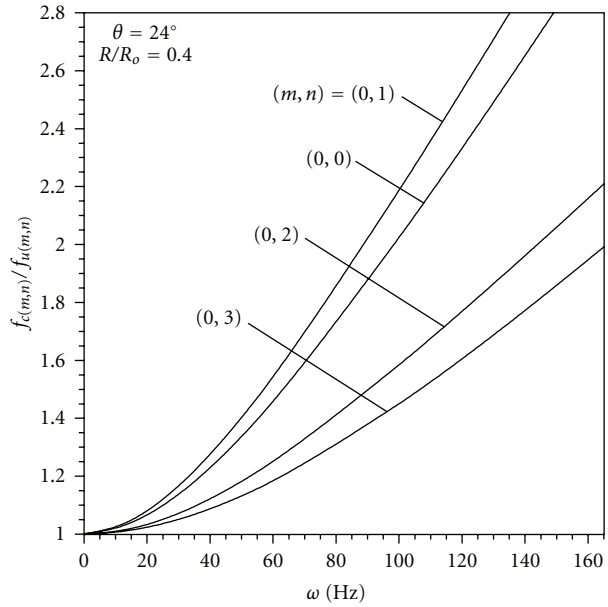

Figure 14: Variations in the four lower dimensionless natural frequencies versus the angular speed ω for a disk with a circumferential crack of angle $\theta = 24^\circ$ at a distance $R/R_o = 0.4$.

4. Conclusions

This study constitutes a primary approach for the vibrational behaviour of a constantly rotating disk with a radial or circumferential crack. The disk is discretised into finite elements, and the crack is considered as nonpropagating and always open. Based on the eigenvalue and harmonic analyses, the natural frequencies, mode shapes, and frequency response due to dynamic loading are yielded. For both crack

orientations, parametric studies are conducted to investigate the sensitivity of the vibrational behaviour to the disk's angular speed and radial crack length or circumferential angle and distance from the disk's centre. The influence of crack characteristics (position, depth, and distance) on the critical speed is also studied. The accuracy of the results is demonstrated through comparisons with numerical results available in the literature and analytical results. It was deduced that for the rotating disk with a radial crack the natural frequency for mode shapes $(0,1)$, $(0,2)$, and $(0,3)$ split into two frequencies. One frequency corresponds to the symmetric mode shapes and the other to the antisymmetric mode shapes. The mode shape $(0,0)$ appears symmetric and possesses a single natural frequency. Natural frequencies of both symmetric and antisymmetric mode shape $(0,1)$ are affected only by high values of radial length. The remaining natural frequencies are sensitive to the changes of radial length. For all considered crack cases in this study, the natural frequencies increase within the considered range of angular speed values. Critical speeds appear for the symmetric and antisymmetric mode shapes $(0,2)$ and $(0,3)$ which decrease as the radial crack length increases. For the rotating disk with a circumferential crack, all the mode shapes are symmetric and have the same form with the corresponding mode shapes of the uncracked rotating disk. Two identical natural frequencies correspond to the mode shapes $(0,1)$, $(0,2)$, and $(0,3)$ while a single natural frequency to the mode shape $(0,0)$. The values of all considered natural frequencies are unaffected by circumferential crack's angle and dimensionless distance. For all considered values of angular speed in this study, the values of natural frequencies for the circumferentially cracked disk are very close to the corresponding values of the uncracked rotating disk. The existing critical speeds for mode shapes $(0,2)$ and $(0,3)$ are very close to those of uncracked rotating disk. Based on the above mentioned conclusions, it is believed that this study can be used as complementary tool for crack detection techniques. Furthermore, this study can be extended to consider the Coriolis effects and very high values of angular speeds. These issues are under investigation and will be the subject of future studies of the authors.

References

[1] S. W. Doebling, C. R. Farrar, and M. B. Prime, "A summary review of vibration-based damage identification methods," *Shock and Vibration Digest*, vol. 30, no. 2, pp. 91–105, 1998.

[2] A. D. Dimarogonas, "Vibration of cracked structures: a state of the art review," *Engineering Fracture Mechanics*, vol. 55, no. 5, pp. 831–857, 1996.

[3] H. Lamb and R. V. Southwell, "The vibrations of a spinning disk," *Proceedings of the Royal Society, London, Series A*, vol. 99, pp. 272–280, 1921.

[4] J. Kirkhope and G. J. Wilson, "Vibration and stress analysis of thin rotating discs using annular finite elements," *Journal of Sound and Vibration*, vol. 44, no. 4, pp. 461–474, 1976.

[5] D. S. Liang, H. J. Wang, and L. W. Chen, "Vibration and stability of rotating polar orthotropic annular disks subjected to a stationary concentrated transverse load," *Journal of Sound and Vibration*, vol. 250, no. 5, pp. 795–811, 2002.

[6] J. Chung, J. E. Oh, and H. H. Yoo, "Non-linear vibration of a flexible spinning disc with angular acceleration," *Journal of Sound and Vibration*, vol. 231, no. 2, pp. 375–391, 2000.

[7] J. Chung, J. W. Heo, and C. S. Han, "Natural frequencies of a flexible spinning disk misaligned with the axis of rotation," *Journal of Sound and Vibration*, vol. 260, no. 4, pp. 763–775, 2003.

[8] J. W. Heo, J. Chung, and K. Choi, "Dynamic time responses of a flexible spinning disk misaligned with the axis of rotation," *Journal of Sound and Vibration*, vol. 262, no. 1, pp. 25–44, 2003.

[9] N. Baddour and J. W. Zu, "Nonlinearly coupled in-plane and transverse vibrations of a spinning disk," *Applied Mathematical Modelling*, vol. 31, no. 1, pp. 54–77, 2007.

[10] S. Bashmal, R. Bhat, and S. Rakheja, "In-plane free vibration of circular annular disks," *Journal of Sound and Vibration*, vol. 322, no. 1-2, pp. 216–226, 2009.

[11] V. Ranjan and M. K. Ghosh, "Transverse vibration of spinning disk with attached distributed patch and discrete point masses using finite element analysis," *International Journal of Engineering, Science and Technology*, vol. 1, pp. 74–89, 2009.

[12] D. P. Rooke and J. Tweed, "The stress intensity factors of a radial crack in a finite rotating elastic disc," *International Journal of Engineering Science*, vol. 10, no. 8, pp. 709–714, 1972.

[13] R. N. L. Smith, "Stress intensity factors for an ARC crack in a rotating disc," *Engineering Fracture Mechanics*, vol. 21, no. 3, pp. 579–587, 1985.

[14] G. A. Schneider and R. Danzer, "Calculation of the stress intensity factor of an edge crack in a finite elastic disc using the weight function method," *Engineering Fracture Mechanics*, vol. 34, no. 3, pp. 547–552, 1989.

[15] M. Shariati, E. Mohammadia, and M. Mahdizaseh Rokhia, "Calculation of stress intensity factor by algebraic emulator based on statistical resultants of FRANC2D in rotary cracked disks," *Journal of Applied Sciences*, vol. 8, no. 16, pp. 2924–2927, 2008.

[16] H. S. Jia and C. W. Lee, "On the vibration of imperfect circular disks," *KSME International Journal*, vol. 12, no. 2, pp. 223–232, 1998.

[17] A. Raman and C. D. Mote, "Experimental studies on the non-linear oscillations of imperfect circular disks spinning near critical speed," *International Journal of Non-Linear Mechanics*, vol. 36, no. 2, pp. 291–305, 2001.

[18] A. L. Gyekenyesi, J. T. Sawicki, and G. Y. Baaklini, "Vibration based crack detection in a rotating disk part 1—an analytical study," Tech. Rep. NASA/TM-2003-212624, NASA, 2003.

[19] A. L. Gyekenyesi, J. T. Sawicki, R. E. Martin, W. C. Haase, and G. Baaklini, "Vibration based crack detection in a rotating disk part 2—experimental results," Tech. Rep. NASA/TM- 2005-212624/PART2, NASA, 2005.

[20] S. H. Hsieh and J. F. Abel, "Comparison of two finite element approaches for analysis of rotating bladed-disk assemblies," *Journal of Sound and Vibration*, vol. 182, no. 1, pp. 91–107, 1995.

[21] K. J. Bathe, *Finite Element Procedures*, Prentice Hall, Upper Saddle River, NJ, USA, 1996.

[22] B. W. Huang and J. H. Kuang, "Mode localization in a rotating mistuned turbo disk with Coriolis effect," *International Journal of Mechanical Sciences*, vol. 43, no. 7, pp. 1643–1660, 2001.

[23] M. Lessen and M. D. Gangal, "Effect of Coriolis acceleration on the vibrations of rotating disks," *Applied Scientific Research*, vol. 22, no. 1, pp. 338–344, 1970.

[24] L. Meirovitch, *Analytical Methods in Vibrations*, Macmillan Company, New York, NY, USA, 1967.

[25] R. C. Yu and C. D. Mote, "Vibration and parametric excitation in asymmetric circular plates under moving loads," *Journal of Sound and Vibration*, vol. 119, no. 3, pp. 409–427, 1987.

[26] P. F. Pai, Y. Oh, and S. Y. Lee, "Detection of defects in circular plates using a scanning laser vibrometer," *Structural Health Monitoring*, vol. 1, no. 1, pp. 63–88, 2002.

[27] G. K. Ramaiah, "Natural frequencies of spinning annular plates," *Journal of Sound and Vibration*, vol. 74, no. 2, pp. 303–310, 1981.

[28] J. Yuan, P. G. Young, and S. M. Dickinson, "Natural frequencies of circular and annular plates with radial or circumferential cracks," *Computers and Structures*, vol. 53, no. 2, pp. 327–334, 1994.

[29] A. Demir and V. Mermertaş, "Natural frequencies of annular plates with circumferential cracks by means of sector element," *Engineering Fracture Mechanics*, vol. 75, no. 5, pp. 1143–1155, 2008.

[30] M. Amabili, *Nonlinear Vibrations and Stability of Shells and Plates*, Cambridge University Press, 2008.

[31] R. V. Southwell, "On the free transverse vibration of a uniform circular disk clamped at its centre and on the effects of rotation," vol. 101, pp. 133–153, 1922.